DIDACTICAL EXPERIMENTS ON GRAVITATIONAL LENSING

Jean Surdej{1}{*}, Sjur Refsdal{2} and Anna Pospieszalska-Surdej{1}
{1}Institut d'Astrophysique, Université de Liège, Avenue de Cointe 5, B-4000 Liège, Belgium
{2}Hamburg Observatory, Gojenbergsweg 112, D-21029, Hamburg-Bergedorf, Germany
{*}also Research Director, Belgian Fund for Scientific Research (FNRS)

ABSTRACT

Because of refractive index variations in the air layers just above the ground, atmospheric lensing may significantly deform our view of distant Earth-objects. Similarly, gravitational lensing perturbs our view of the distant Universe and affects our physical understanding of various classes of extragalactic objects. After recalling the basic principles underlying the formation of atmospheric and gravitationally lensed mirages, we describe a simple optical lens experiment which accounts for all types of image configurations observed among presently known gravitational lens systems.

The didactical experiments proposed in this contribution and most of the figures are adapted from Surdej (1990), Refsdal and Surdej (1992, 1994) and Surdej, Refsdal and Pospieszalska-Surdej (1993, 1995).

1. Atmospheric Lensing

Figure 1 (left), gives a schematic representation of the light ray paths from a distant car (the air close to the ground is hotter than at upper levels). Because air refraction always leads to a bending of light rays towards regions of colder (i.e. more dense) air, several lower and somewhat deformed images of a distant source may result (cf. the car lights in this first example). Figure 1 (right) represents the multiple images of the lights from a distant car, as photographed with a 200 mm focal length camera, along the US 60 road between the towns of Magdalena and Datil near the Very Large Array (New Mexico, USA) on the night of 11 January 1989. The distance between the car and the observers is estimated to be about 10 miles.

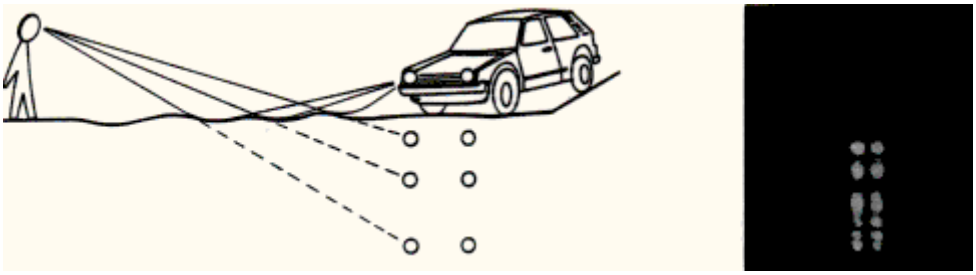

Figure 1: Propagation of light rays above a heated ground between a distant car and an observer (left) and formation of multiple images due to atmospheric lensing (right)

Such terrestrial mirages, usually made of two single images (cf. Figure 2), can actually be seen almost everyday. In addition to significantly affect our view (image deformation, multiplication, etc.) of distant resolved Earth-sources (cf. the resolved images in Figures 1 (right) and 2 (right)), atmospheric lensing is also often responsible for the light amplification of distant unresolved objects located along straight and long roads or across flat countrysides. This was the case, for instance, when looking directly with our naked eyes at the atmospheric mirage illustrated in Figure 1. The car lights then just appeared to consist of a very bright spot ... abnormally bright for a car located at a distance of approximately 10 miles from the observers. Figure 2 (right) illustrates the formation of one lower, inverted and somewhat deformed image of a distant car photographed along the North Panamericana highway between the towns of Pichidangui and La Serena in Chile (2 December 1987).

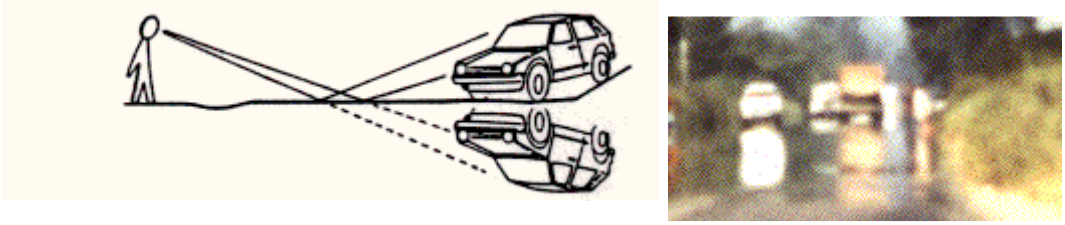

Figure 2: Propagation of light rays above a heated ground (left) and formation of two (direct and inverted) images of the distant car due to atmospheric lensing (right)

Figures 3 and 4 illustrate two other examples of atmospheric lensing. They correspond to two different views of the north-south arm of the Very Large Array (VLA) at the National Radio Astronomical Observatory (Socorro, New Mexico, USA). On that early morning of 17 January 1989, the air warmed up by the rising sun was hotter than the ground, leading to the formation of upper-type mirages (cf. the very distinct upper image for the antenna at right in Figure 4).

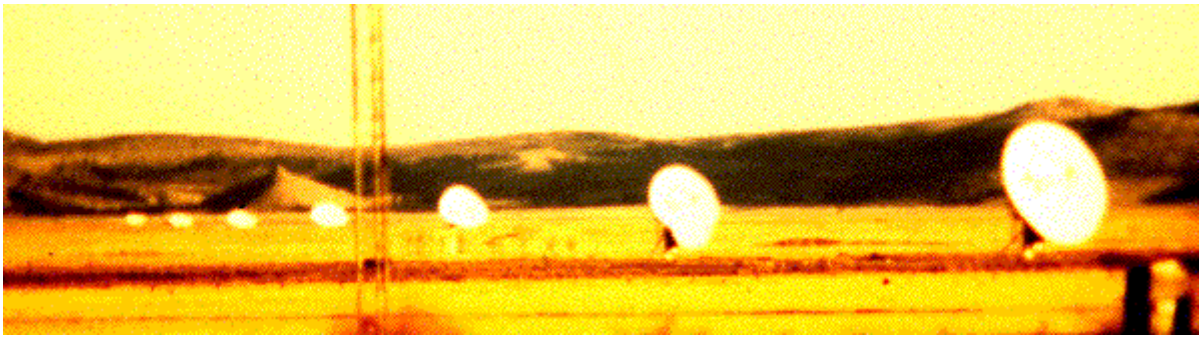

Figure 3: Distorted images of antenna along the north-south arm of the Very Large Array (NRAO, New Mexico) in the early morning of 17 January 1989

Given a distribution n(z) for the air refractive index as a function of the vertical height z, it is easy to construct numerically the resulting mirage of a distant source as seen by an observer. This exercise could be the subject of a laboratory in physics for high school students having some basic knowledge in programming (cf. BASIC or FORTRAN). For those students interested in the numerical simulation of such atmospheric mirages, we give hereafter a more thorough physical description of the bending of light rays due to atmospheric lensing (Exercise 1).

Figure 4: Distorted and multiple images of some of the antenna of the Very Large Array (NRAO, New Mexico) on 17 January 1989. Note the upper, nicely detached image for the antenna at right

1.1 Exercise 1: Physical description of atmospheric lensing

In order to understand in more details the light propagation across a plane parallel atmosphere whose refractive index is affected by a vertical gradient dn/dz, we may apply Fermat's principle according to which the path(s) followed by light between two given points is that (or those) which correspond(s) to an extremum in the propagation time, i.e.

$$\delta\left(\int_o^s \frac{1}{v}\, ds\right) = 0\ , \qquad (1.1)$$

where $ds=\sqrt{dx^2 + dz^2}$ represents an infinitesimal element along the light trajectory and v=c / n, the velocity of light in the medium with a refractive index n(z) (see Fig. 5). It is easy to show, by means of the Euler-Lagrange equation, that the variational equation (1.1) simply reduces to Descartes's law

$$n(z)\cos(i(z)) = K, \qquad (1.2)$$

where K is a constant and *i*(z) represents the angle between the tangent to the light ray and the horizontal direction. It is then straightforward to derive the expression for the small angle increment δi of the ray between two neighbouring points whose abscissae are x and x+dx. For a small but finite value of dx and small inclination angle *i*, we find with a good approximation that

$$\delta i = \frac{(dn/dz)\, dx}{n(z)} \qquad (1.3)$$

This relation is very useful in order to construct numerically the trajectory of light rays across an atmosphere characterized by a refractive index distribution n(z). In doing so, one finds that under special circumstances (cf. specific refractive index distributions n(z), source distance, etc.) there may exist several geodesics between the source and the observer, resulting in the possible formation of multiple images. It is also interesting to note that because of the difference in the geometric lengths and light velocities (c / n(z)) along two geodesics, there will generally be a delay between the arrival times of a signal from the source (cf. a hypothetical light flash) as seen by a distant observer. This time delay depends of course on the refractive index distribution n(z) and also on the absolute distance between the source and the observer.

Finally, let us remark that because atmospheric lensing preserves surface brightness, just as in the case of gravitational lensing, the amplification of a mirage luminosity is simply given by the ratio of the solid angle of the observed (lensed) image to that of the (unlensed) source. Therefore, in addition to affecting significantly our view (image deformation, multiplication, etc.) of distant resolved Earth-sources, atmospheric lensing is also often responsible for the light amplification of distant unresolved objects located along straight and long roads or across flat countrysides.

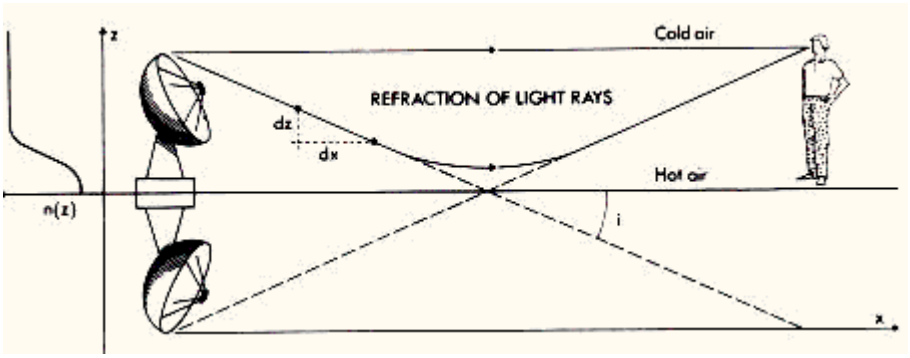

Figure 5: Formation of atmospheric mirages across an atmosphere characterized by a refractive index distribution n(z), as shown along the left horizontal axis

As we shall see in the remainder, there exist quite a few other similarities between atmospheric and gravitational lensing.

2. Gravitational Lensing

During the elaboration of his theory of General Relativity, Einstein (1915) predicted that a massive object curves the spacetime in its vicinity and that any particle, massive or not (cf. the photons), will move along the geodesics of this curved space. He showed that a light ray passing at a distance ξ from an object characterized by an axially symmetric mass distribution $\boldsymbol{M}(\xi)$ (see Figure 1) will undergo a total deflection angle $\hat{\alpha}(\xi)$, expressed in radian by means of the relation

$$\hat{\alpha}(\xi) = \frac{4\,G}{c^2}\frac{\boldsymbol{M}(\xi)}{\xi}, \qquad (2.1)$$

where G stands for the gravitational constant and c for the velocity of light. Adopting a given mass distribution (e.g. a constant mass $\boldsymbol{M}(\xi) = \boldsymbol{M}$ in order to characterize a point-like object, the disk of a spiral galaxy, etc.), it is then trivial to construct an optical lens that deflects light rays accordingly, thus enabling us to study very simply in the laboratory the lensing properties of black holes, stars, quasars, galaxies, etc. as they exist in the Universe. We discuss this in greater details in the next section.

Before discussing the optical gravitational lens experiment, we wish to state that a sufficient condition for a gravitational lens to produce multiple images of a background source is simply that its surface mass density $\boldsymbol{\Sigma}(\xi)$ exceeds the critical density $\boldsymbol{\Sigma}_c$, which only depends on the relative distances D_{od}, D_{os} and D_{ds}, between the observer (O), the deflector (D) and the source (S) (cf. Equation (2.4)-(2.6)). It is also very easy to show that in the case of a perfect alignment between a source, an axially symmetric deflector and an observer, the latter will see the background source as a ring of light (the so-called Einstein ring) which angular radius $\boldsymbol{\Theta}_E$ is proportional to the square root of the mass of the deflector (cf. Equation (2.7)). For those students who are very curious, we propose hereafter the derivation of the quantities $\boldsymbol{\Sigma}_c$ and $\boldsymbol{\Theta}_E$ (Exercise 2).

2.1 Exercise 2: Condition for multiple imaging and angular radius of the Einstein ring

In the case of perfect alignment between a source (S), an axially symmetric deflector (D) and an observer (O) (see Fig. 1), we easily see that, with the exception of the direct ray propagating from the source to the observer, the condition for any other light ray to reach the observer is

$$\frac{\theta}{D_{ds}} \simeq \frac{\hat{\alpha}_o}{D_{os}}, \qquad (2.2)$$

as obtained from the direct application of the sine rule in the triangle SXO and assuming that the angles $\boldsymbol{\Theta}$ and $\hat{\alpha}_c$ remain very small. Of course, this will also be true if the real deflection angle $\hat{\alpha} \geq \hat{\alpha}_c$ since it will then be always possible to find a light ray with a greater impact parameter ξ such that Eq. (2.2) is fulfilled. Expressing the angle $\boldsymbol{\Theta}$ between the direct ray and the incoming deflected ray as

$$\theta \simeq \frac{\xi}{D_{od}}, \qquad (2.3)$$

and making use of Eqs. (2.1) and (2.2), we may thus rewrite the above condition as follows

$$\Sigma(<\xi) \geq \Sigma_c, \qquad (2.4)$$

i.e. the average surface mass density of the lens

$$\Sigma(<\xi) = \frac{M(\xi)}{\pi \xi^2}, \qquad (2.5)$$

evaluated within the impact parameter ξ, must simply exceed the critical surface mass density Σ_c, defined by

$$\Sigma_c = \frac{c^2 \, D_{os}}{4 \, \pi \, G \, D_{od} \, D_{ds}}. \qquad (2.6)$$

Let us note that the latter quantity is essentially determined by the distances between the source, the deflector and the observer.

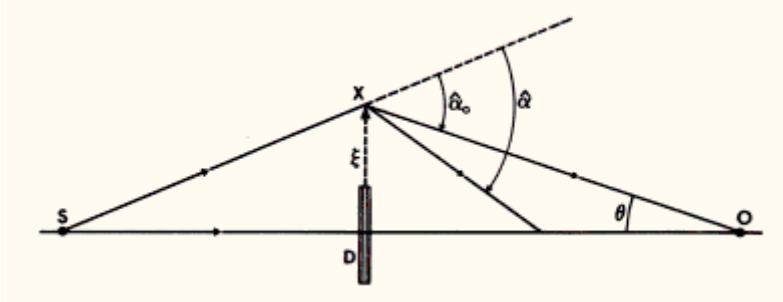

Figure 1: On the condition for an observer O to see a light ray from a distant source S, deviated by a deflector D so that more than one image can be seen. Note that O, D and S are perfectly co-aligned and that axial symmetry is assumed. No scale is respected in this diagram

Although the above reasoning essentially applies to a static Euclidian space, Refsdal (1966) has shown that it also remains valid for Friedmann, Lemaître, Robertson, Walker (FLRW) expanding universe models, provided that D_{od}, D_{os} and D_{ds} represent angular size distances. Adopting typical cosmological distances for the deflector (redshift $z_d \simeq 0.5$) and the source ($z_s \simeq 2$), we find that $\Sigma_c \simeq 1\ g/cm^2$.

Substituting $M(\xi)$ and ξ in Eq. (2.5) with a typical mass M and a radius R for the deflector, we have listed in Table 1 values for the ratio $\Sigma(<R)/\Sigma_c$ considering a star, a galaxy and a cluster of galaxies located at various distances.

Deflector	M	D_{od}	R	$\Sigma(<R)\ /\ \Sigma_c$	θ_E	$\xi_E = \theta_E\ D_{od}$
Star	$1\ M_\odot$	10^4 pc	$2\ 10^{-8}$ pc	$2\ 10^6$	$6\ 10^{-4}$"	$3\ 10^{-5}$ pc
Star	$1\ M_\odot$	10^9 pc	$2\ 10^{-8}$ pc	$2\ 10^{11}$	$2\ 10^{-6}$"	10^{-2} pc
Galaxy core	$10^{12}\ M_\odot$	10^9 pc	$5\ 10^3$ pc	4	2"	10^4 pc
Cluster core	$10^{14}\ M_\odot$	10^9 pc	10^6 pc	1	20"	10^6 pc

Table 1: Ratio of the average Σ(<R) and critical Σ_c surface mass densities, angular (Θ_E) and linear (ξ_E) radii of the Einstein ring for different values of the mass M, distance D_{od} and radius R of the deflector, assuming that D_{od} = 2 x D_{od}

(1 par sec = 1 pc = 3.262 light years = 3.086 10^{18} cm)

We see that only stars and very compact, massive galaxies and galaxy clusters, for which $\Sigma(<R)/\Sigma_c \geq 1$, constitute promising `multiple imaging' deflectors.

In the case of axial symmetry, it is clear that in the presence of an efficient deflector, an observer located on the symmetry axis will actually see a ring (the so-called 'Einstein ring', cf. Fig. 10) of light from a distant source. Combining Eqs. (2.1)-(2.3), the angular radius of this ring may be conveniently expressed as

$$\theta_E = \sqrt{\frac{4\ G\ M(\leq D_{od}\theta_E)\ D_{ds}}{c^2\ D_{od}\ D_{os}}}. \qquad (2.7)$$

We have also listed in Table 1 typical values of Θ_E for different types of deflectors located at various distances.

As we shall see in the optical gravitational lensing experiment, the value of Θ_E derived above is very important because it can usually be used to estimate the angular separation between multiple lensed images in more general cases where the condition of a perfect alignment between the source, deflector and observer is not fulfilled or even for lens mass distributions which significantly depart from the axial symmetry. Knowing that angular size distances are inversely proportional to the Hubble constant H_o, observed image separations ($\simeq 2\Theta_E$) can therefore lead to the value of M/D_{od}, or to the value of M times the Hubble constant H_o, if the redshifts z_d and z_s are known. This is the simplest and most direct astrophysical application of gravitational lensing. We see from Table 1 that for a source and a lens located at cosmological distances ($z_d \simeq 0.5$ and $z_s \simeq 2$), the angle Θ_E can vary from micro-arcsec (stellar deflection) to arcsec (galaxy lensing), and up to some tens of arcsec in the case of cluster lenses. Let us also finally note that the condition (2.4) for a deflector to produce multiple images of a lensed source turns out to be usually applicable, even when there is no axial symmetry.

3. The Optical Gravitational Lens Experiment

For didactical purposes, it is very useful to construct and use optical lenses that mimic the deflection of light rays as derived in Eq. (2.1) for the case of axially symmetric gravitational lenses. Such optical lenses should of course be rotationally symmetric, flat on one side (for simplicity) and have, on the other side, a surface determined in such a way that rays characterized by an impact parameter ξ gets deflected by the angle

$$\epsilon(\xi) = \hat{\alpha}(\xi)$$

(see Eq. (2.1) and Fig. 1). Optical lenses simulating the light deflection properties due to a point mass (cf. a black hole), a singular isothermal sphere and a spiral galaxy have been manufactured by the authors (see Figs. 2 and 3). A detailed description of their shapes is proposed in exercise 3.

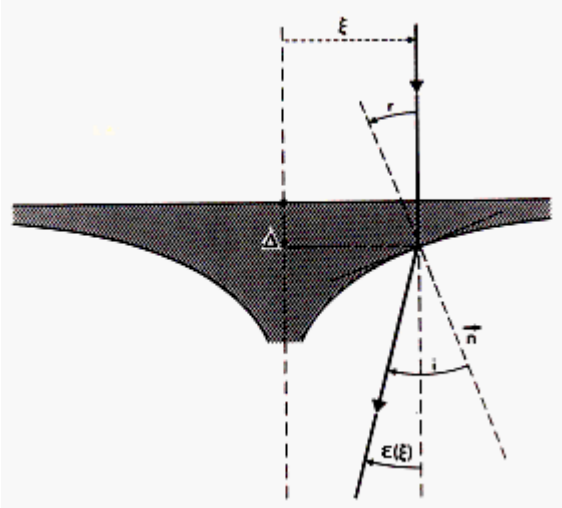

Figure 1: Deflection of a light ray passing through an axially symmetric optical lens

3.1. Exercise 3: Shapes of axially symmetric optical lenses

Applying Descartes's law (cf. Eq. (1.2)) to the ray depicted in Fig. 1 and assuming that the angles (r and i) between the normal $\vec{n}$ to the optical surface and the incident and refracted rays are very small, we may write the relation

$$n = \frac{sin(i)}{sin(r)} \simeq \frac{i}{r}, \qquad (3.1)$$

where n represents here the refractive index of the lens with respect to the air. Furthermore, since we have

$$i = \epsilon(\xi) + r = \frac{4GM(\xi)}{c^2\xi} + r, \qquad (3.2)$$

and that the tangent to the optical surface at the point (ξ, Δ) is merely given by (see Fig. 1)

$$\frac{d\Delta}{d\xi} = -r, \qquad (3.3)$$

it is straigtforward to derive the shape of a lens by means of the following differential equation

$$\frac{d\Delta}{d\xi} = \frac{-4GM(\xi)}{(n-1)c^2\xi}. \qquad (3.4)$$

3.1.1. The optical point mass lens

By definition, the mass ***M*** of a point lens model is concentrated in one point such that we have $\boldsymbol{M}(\xi)=\boldsymbol{M}$ It is then simple to solve Eq. (3.4) and derive the thickness $\Delta(\xi)$ of the corresponding optical lens as a function of the impact parameter ξ. We find that

$$\Delta(\xi) = \Delta(\xi_o) + \frac{2R_{sc}}{n-1} ln(\frac{\xi_o}{\xi}), \qquad (3.5)$$

Where

$$R_{sc} = 2GM/c^2$$

represents the Schwarzschild radius of the compact lens. In practice, the point

$$(\xi_o, \Delta(\xi_o))$$

is chosen in order to specify a given thickness (e.g. $\boldsymbol{\Delta}(\xi_o)$ = 1 cm) for the optical lens at a selected radius (e.g. ξ_0 = 15 cm). The resulting shape of such an optical 'point mass' lens is illustrated in Fig. 2a. It looks very much like the foot of some glasses of wine which, therefore, have been commonly used in the past by some astronomers to simulate lensing effects. A realistic 'point mass' lens, made of plexiglas-like material (refractive index n = 1.49 and a diameter of 30cm has been manufactured by the authors for the particular value of R_{sc}=0.3cm, corresponding to the Schwarzschild radius of one third of the Earth mass (see Fig. 3, left).

Figure 2: Several examples of axially symmetric optical lenses simulating the light deflection properties due to a point mass (a), a SIS galaxy (b) and a spiral galaxy (c)

Figure 3: Examples of a 'point mass' (left) and a 'spiral galaxy' (right) optical lens produced by the authors. We have used these particular lenses, made of plexiglas-like material (n = 1.49, 30 cm in diameter), to simulate the formation of multiple images of a distant source. The optical gravitational lens experiment is described in section 4.

3.1.2. The SIS optical lens

For the case of a singular isothermal sphere (hereafter SIS) lens model, it is well known that the mass of such a galaxy increases linearly with the impact parameter ξ, *i.e.* $M(\xi)\ \alpha\ \xi$. We may thus rewrite Eq. (3.4) in the form

$$\frac{d\Delta}{d\xi} = -K, \qquad (3.6)$$

where K represents a positive constant. Integration of the above equation leads to the solution

$$\Delta(\xi) = \Delta(\xi_o) + K(\xi_o - \xi). \qquad (3.7)$$

The shape of the resulting SIS lens is thus merely an axially symmetric cone as illustrated in Fig. 8b.

3.1.3. The 'spiral galaxy' optical lens

Given the exponential surface mass density

$$\Sigma(\xi) = \Sigma_o \exp(-\frac{\xi}{\xi_c}), \qquad (3.8)$$

which describes reasonably well the mass distribution of a spiral galaxy disk having a characteristic size ξ_c, we may derive the mass distribution $M(\xi)$ of such a deflector by means of the relation

$$M(\xi) = 2\pi \int_0^{\xi} \Sigma(\xi')\xi' d\xi'. \qquad (3.9)$$

Integration of this last expression leads immediately to the result

$$M(\xi) = 2\pi \xi_c^{\,2} \Sigma_o [1 - \exp(-\frac{\xi}{\xi_c})(\frac{\xi}{\xi_c} + 1)]. \qquad (3.10)$$

Inserting this result into Eq. (3.4) and performing the integration, we find that

$$\Delta(\xi) = \Delta(\xi_o) + \frac{8\pi G \xi_c^{\,2} \Sigma_o}{(n-1)c^2}[\ln(\frac{\xi_o}{\xi}) - \exp(\frac{-\xi}{\xi_c}) + \exp(\frac{-\xi_o}{\xi_c}) + \int_{\frac{\xi_o}{\xi_c}}^{\frac{\xi}{\xi_c}} \frac{\exp(-z)}{z} dz]. \quad (3.1$$

The general shape of a 'spiral galaxy' optical lens is illustrated in Fig. 2c. A 30 cm diameter 'spiral galaxy' lens, produced by the authors, is shown in Fig. 3 (right). This lens is characterized by the following physical parameters: an equivalent Schwarzschild radius of one third of the Earth mass, i.e.

$R_{sc} = 2GM(\xi \to \infty)/c^2 = 4\pi G \xi_c^{\,2} \Sigma_o / c^2 = 0.3 \ cm$

(see Eq. (3.10)),

$\xi_c = 2.0\ cm, \quad \xi_o = 15\ cm \ and \ \Delta(\xi_o) = 0.7\ cm$

4. Setup of the optical gravitational lens experiment

In order to simulate the formation of lensed images by a given mass distribution (point mass, etc.), we have used the optical setup that is shown in Fig. 1.

Figure 1: Setup of the optical gravitational lens experiment

A compact light source is located on the left side (not clearly seen), then comes the point mass optical lens (cf. Fig. 3, in section 3, left) that deflects the light rays very nearly as a black hole having one third of the Earth mass. Behind the lens, we find a white screen with a small hole at the center (pinhole lens). Further behind, there is a large screen on which is projected the lensed image(s) of the source (the Einstein ring, in this case) as it would be seen if our eye were located at the position of the pinhole. In the example illustrated here, the pinhole is set very precisely on the optical axis of the gravitational lens so that the source, the lens and the pinhole (observer) are perfectly aligned. Some smoke in this experiment reveals the existence of a bright `pseudo- focal' line along the optical axis. Intersection of this line with the pinhole screen thus consists of a bright white spot (cf. Figure 2a). Note that the bright regions seen on the lens in Fig. 1 are essentially caused by scattered light. Let us now produce a second type of gravitational lens mirage: as we move the pinhole very slightly away from the symmetry axis (Fig. 2b), the Einstein ring breaks in two images which angular separation remains comparable with the diameter of the Einstein ring (Fig. 2c).

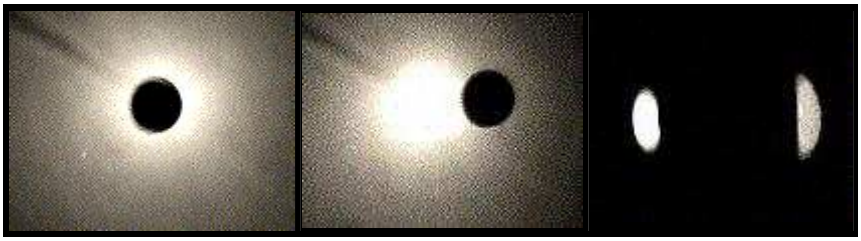

Figure 2: Optical gravitational lens experiment: in this first experiment used to simulate the gravitational deflection of light rays by a point mass lens model, the pinhole (observer) is set very precisely on the optical axis of the gravitational lens so that the source, the lens and the observer are perfectly aligned (left). The resulting image is an Einstein ring (see Fig. 1). As the pinhole is moved slightly away from the symmetry axis (middle), the Einstein ring breaks up in two images (right).

The effects of a typical non symmetric (singular) gravitational lens may be simulated by simply tilting the optical lens around its vertical axis. In this case (see Fig. 3a), the bright (focal) line along the optical axis which existed in the symmetric configuration (cf. Fig. 2a) has changed into a two dimensional caustic surface, a section of which is seen as a diamond shaped caustic (made of four folds and four cusps) in the pinhole plane. As a result, the Einstein ring that was observed in the symmetric case has now split up into four lensed images (Fig. 3b). Such a configuration of four lensed images always arises when the pinhole (observer) lies inside the diamond formed by the caustic. Let us immediately note that such caustics constitute a generic property of gravitational lensing, the focal line in the symmetric configuration being just a degenerate case. Fig. 3d shows the merging of two of the four images into one, single, bright image when the pinhole approaches one of the fold caustics (Fig. 3c). Just after the pinhole has passed the fold caustic (see Fig. 3e), the two merging images have totally disappeared (Fig. 3f).

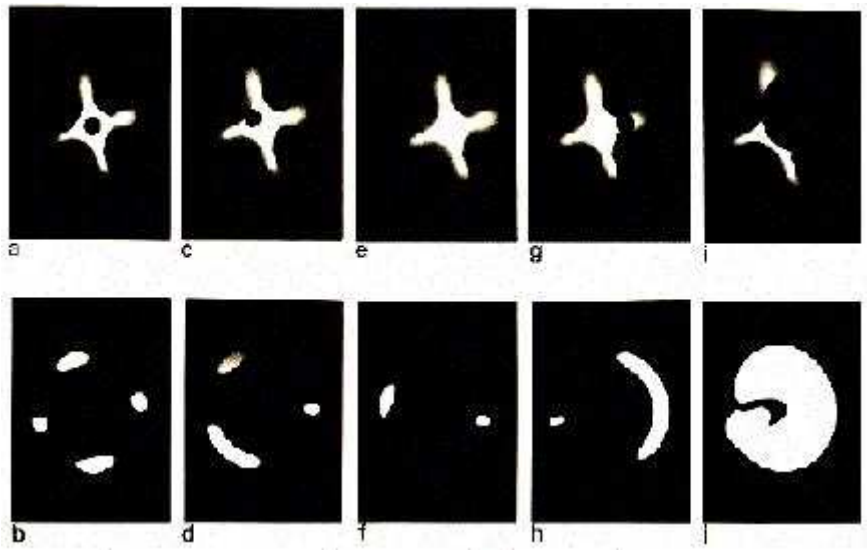

Figure 3: The optical gravitational lens experiment for the case of an asymmetric, singular deflector (see text)

A particularly interesting case occurs when the pinhole (observer) is located very close to one of the cusps (cf. Fig. 3g). Three of the four previous images have then merged into one luminous arc, whereas the fourth one appears as a faint counterimage (Fig. 3h). For large sources that cover most of the diamond shaped caustic (Fig. 3i), an almost complete Einstein ring is observed (Fig. 3j), although the source, lens and observer are not perfectly aligned and the lens is still being tilted. In this last experiment, the increase of the source size has been simulated by enlarging the pinhole radius by a factor 4. In order to show that this is a correct simulation, one may consider the pinhole and the screen behind it as a camera. It is then clear that an increase in the size of the pinhole leads to a larger and less well focused image of the compact source, corresponding indeed to an increase in the source size. A more detailed and rigorous analysis does confirm this result.

In Table1, we are presenting known gravitational lens systems which display image configurations similar to the generic ones simulated in the gravitational lens experiment.

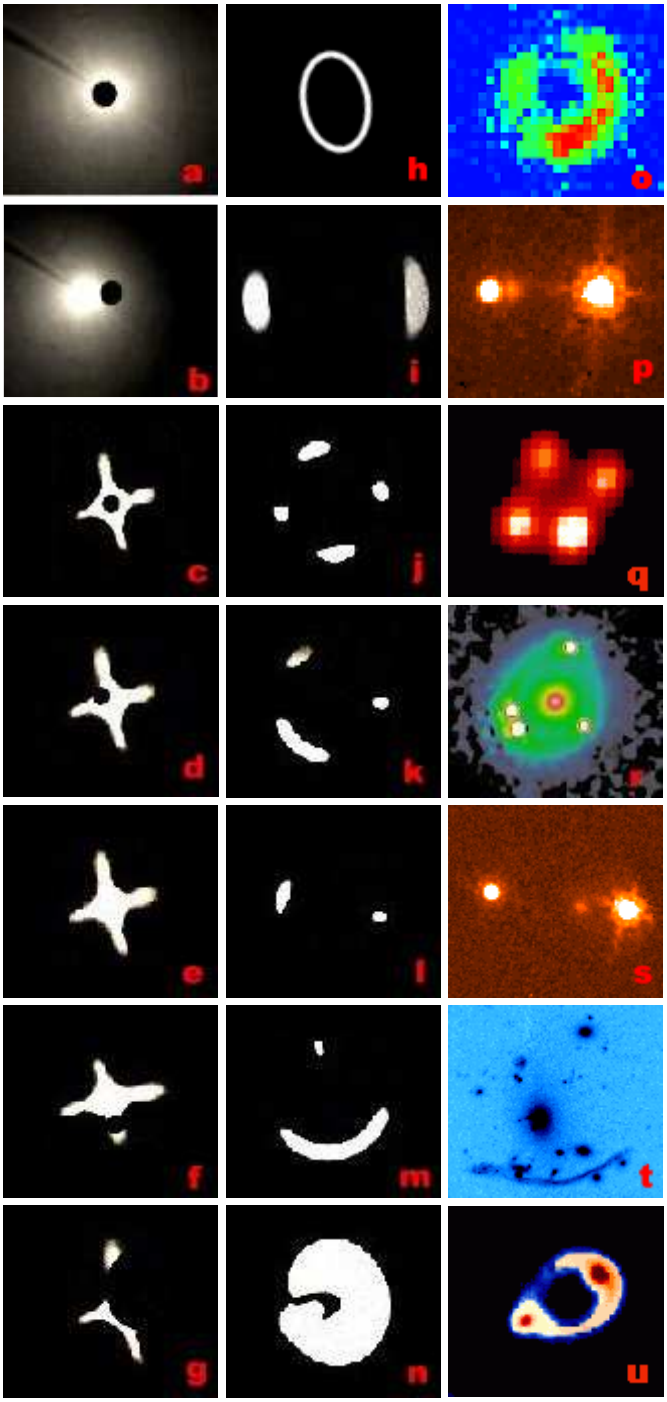

Table 1: Figures a-g represent the light from a distant source that is redistributed over the pinhole screen by symmetric (a-b) or an asymmetric (c-g) optical lens and for various positions of the pinhole (observer). Figures h-n illustrate the corresponding lensed images projected on the large screen located behind the pinhole screen and Figures o-u display known examples of multiply imaged sources (0047-28078), 1009-0252, H1413+117, PG1115+080, HE1104-1805, Abell 370 and MG1131+0456). Images (p), (r), (s) and (t) were obtained using the Hubble Space Telescope, the other ones using ground-based facilities (ESO and VLA/NRAO). Courtesy of the European Southern Observatory (ESO), the Space Telescope Science Institute (STScI) operated for NASA by AURA and the Very Large Array (National Radio Astronomy Observatory).

This optical gravitational lens experiment may also be used to simulate the formation of multiple giant luminous arcs and arclets seen near massive foreground galaxy clusters. In order to do so, we may simply replace the single pinhole screen by a cardboard perforated with multiple pinholes. In the absence of light deflection (i.e. by simply removing the optical lens), direct (non distorted) images of the circular background galaxies would be seen by an observer, alike those projected on the distant white screen (Fig. 4, left).

Figure 4: Giant luminous arcs and arclets (middle and right) resulting from the gravitational lens distortion of background galaxies (left) by a foreground cluster

When inserting the optical lens between the light source and the multiple pinholes screen, images of the background galaxies get distorted (arclets) and/or transformed into multiple images, including giant luminous arcs (see Figs. 4 middle and right as possible examples). While covering the pinholes with various transparent colored filters, the distorted background galaxies look very much like those observed with the Hubble Space Telescope around the foreground galaxy cluster Abell 2218 (see HST press release). More generally speaking, the image configurations illustrated in Figs. 3a-j and 2b-c are all found among the observed gravitational lens systems accessible on one of our web pages http://vela.astro.ulg.ac.be/themes/extragal/gravlens/bibdat/engl/glc_homepage.html. It is of course obvious that if our optical lens would have been constructed non-singular in the center (cf. the 'spiral galaxy' optical lens shown in Fig. 3, section 3, right), we would have seen an additional image formed in the central part of the lens. For most of the known lenses with an even number of observed images, it may well be that a black hole resides in the center of the lens. The presence of a compact core could also account for the "missing" image since then the very faint image expected to be seen close to, or through the core, would be well below the detection limits that are presently achievable.

5. Other Examples of Caustics and Multiple Imaging

5.1 Gravitational lensing and the wine glass experiment

The formation of multiple images of a distant quasar by the gravitational lensing effects of a foreground galaxy may be very simply, and faithfully, accounted for by the wine glass experiment described below.

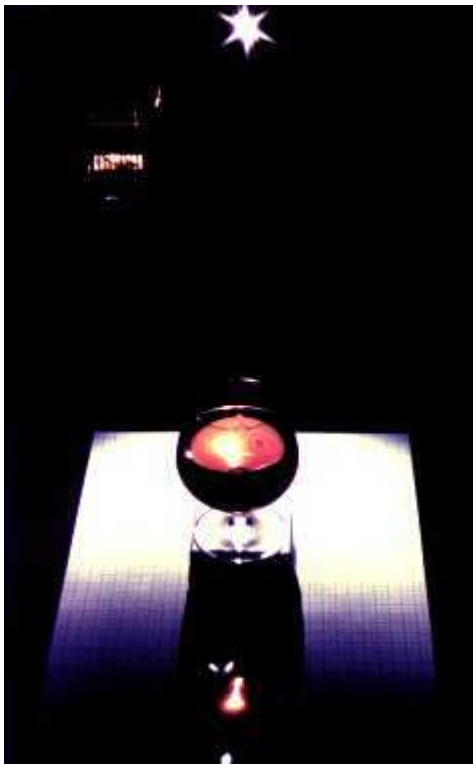

Figure 1: The wine glass experiment. A bright compact light source is used as a distant quasar. The wine glass set on the table (cf Figure 2) distorts the light rays from the quasar and produces a caustics having a triangular shape (see the enlargment in Figure 3). In order to see the multiple images from the distant "quasar", put the glass at the very edge of the table and one of your eyes around the caustics (see text)

In order to successfully make this experiment, please use as the quasar light source a candle, or a bright compact light source as shown in Figure 1. This light source is set at a typical distance of several meters, and somewhat higher, from a table on which a glass full of wine is placed. Like a gravitational lens, the wine glass distorts the background field. This space distortion is very well seen through the glass in Figure 2. Because of the presence of the wine glass, the distribution of light on the table is no longer uniform (see Figure 1). Just behind the glass, higher concentrations of light may be seen at some locations in the form of a caustics (i.e. the intersection of a three-dimensional caustics with the plane of the table). The latter is, in the present case, approximately triangular. The three sides and summits of this triangular caustics are named folds and cusps, respectively.

Figure 2: When looking through the wine glass, the distortion of the background field (millimetric paper) by the lens is very conspicuous

A blow up of this caustics is shown in Figure 3. The folds result from the envelope of pairs of tangent light rays from the candle. As a result, an observer setting his eye on a fold will see a pair of merging images from the distant quasar. Three merging images will be seen at the location of a cusp. In order to be able to put your eye at various locations with respect to the caustics, it is recommended to put the glass at the very edge of the table. You may then also observe that the total number of images increases by two when your eye

crosses a fold from outside to inside the caustics. Figure 4 shows a photograph made with a camera set up at the center of the caustics. Up to 9 different images of the compact light source are visible. As an exercise, draw the various diagrams showing the multiple image configurations of the background light source for different positions of your eye with respect to the caustics (folds and cusps) and compare them with the multiple image configurations observed for the known cases of multiply imaged quasars (a gallery of pictures illustrating various cases of multiply imaged quasars is available via the URL: http://www.aeos.ulg.ac.be/GL/candidates.php.
Note that the formation of caustics of light is a very generic feature in nature. It arises whenever a foreground object (cf. the wine glass in the above experiment, a galaxy acting as a gravitational lens, the wavy interface between air and water in a swimming pool, on a lake, etc.) distorts the propagation of light rays from a distant light source. For instance, for each pair -among the billions- of quasars and galaxies that exist in the Universe, a more or less complex three dimensional caustics is formed behind each galaxy. Whenever an observer lies close to such a caustics, the former sees multiple images of the distant quasar. Due to the relative motion between the quasar, the lensing galaxy and the observer, this phenomenon does not last for ever. It can be shown that the typical lifetime of a cosmic mirage involving a quasar and a lensing galaxy is of the order of 20 million years.

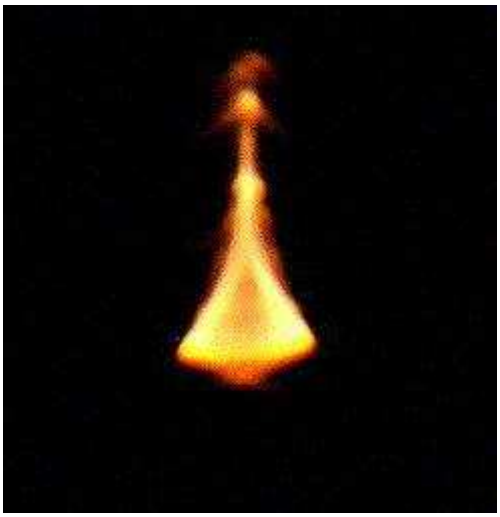

Figure 3: Enlargment of the triangular caustics visible in Figure 1. The caustics results from the redistribution of light rays emitted from the "quasar" by the wine glass

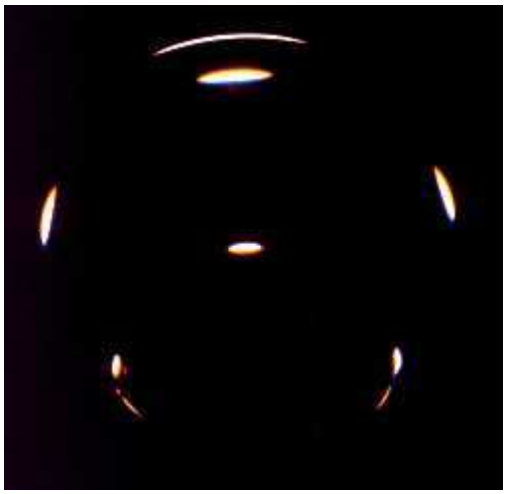

Figure 4: Multiple images of the compact light source seen by the objective of a photographic camera placed near the center of the caustics

5.2 Multiple imaging as seen by whales and sharks

As already stated in the previous section, because of the wind, the interface between the air and the water in a swimming pool, on a lake, on a sea, etc., is wavy and as a result, the propagation of light rays from a distant source (cf. the sun, the moon, etc.) gets distorted after entering water. Here also, complex caustics are formed and Figure 5a reproduces a view of such caustics projected on the body of a swimmer in a pool. Figure 5b illustrates also very well the caustics projected on the body of a whale, as drawn by the famous american painter Miller. There is consequently no doubt that, whenever one of the eyes of a whale crosses the folds (resp. the cups) of the complex caustics, the sun, the moon ... appear to them in the form

of, continuously moving and changing, multiple images. Such multiple images, seen by real sharks inside the large pool at Sea World (Orlando), have been photographed and are reproduced in Figures 6a and 6b.

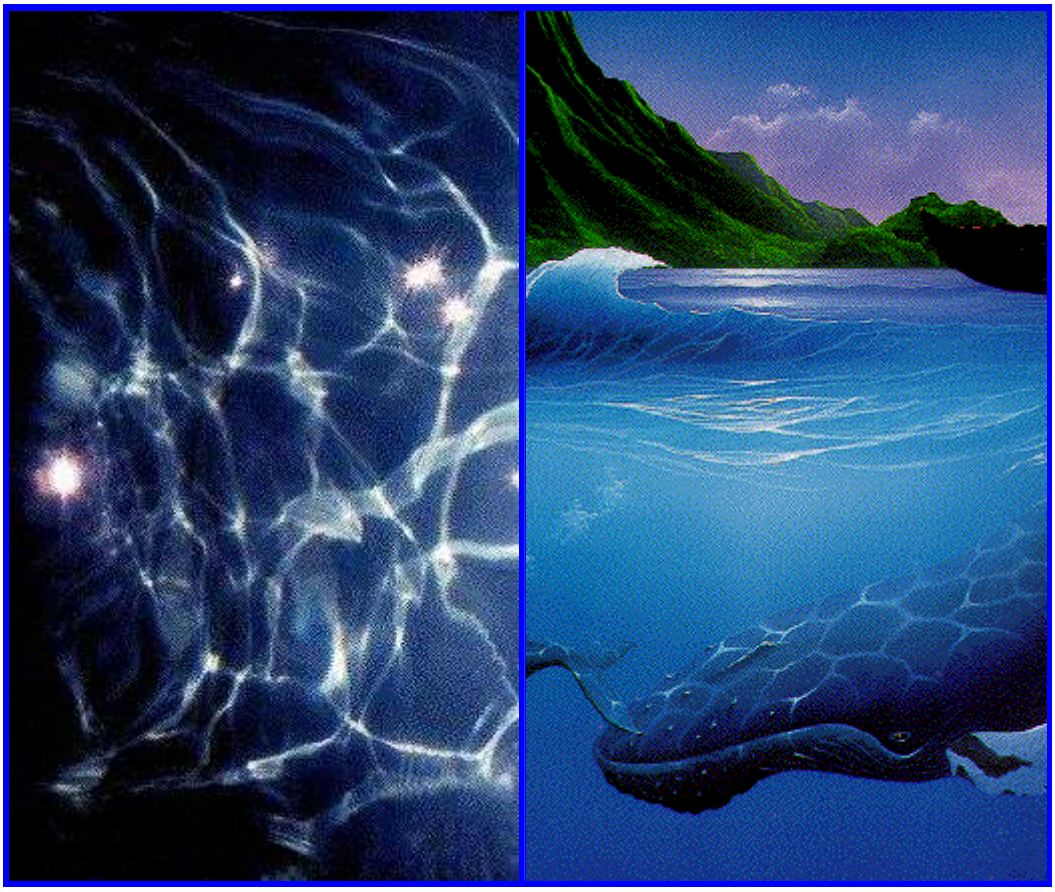

Figure 5: Caustics of light projected on the bottom of the swimming pool (left), and on the body of a whale, as painted by Miller (right). The sun (left) and moon (right) light acts in these case as the distant light source.

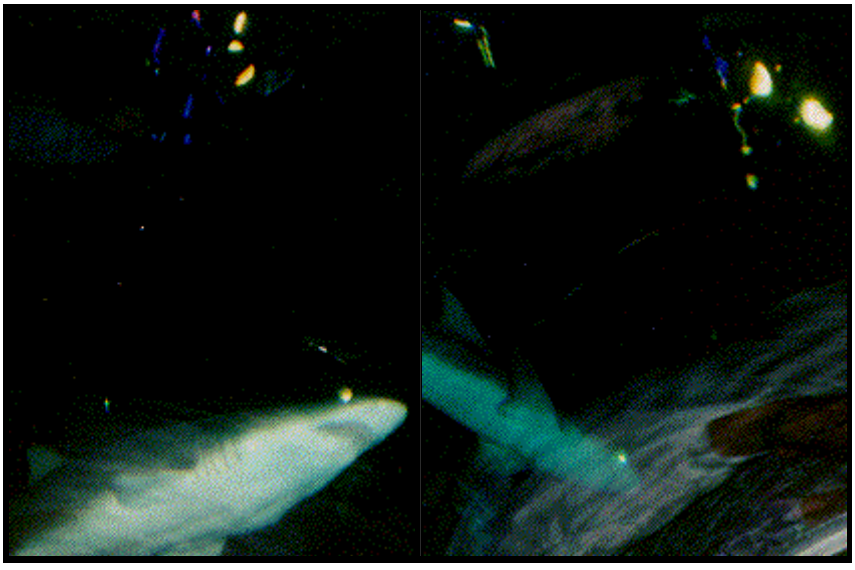

Figure 6: Multiple images seen by sharks in the large pool at Sea World (Orlanda, Florida).

5.3 Multiple imaging at the House of Mirrors

Finally, it is fun to observe multiple images of human beings at the House of Mirrors, available during most of the big city fairs. Such mirages are produced by curved mirrors which distort light rays emitted from the surroundings. Several photographs taken during the Liège october fair in 1989 are reproduced in Figures 6a and 6b.

Figure 7: Multipe images of an astronomer's daugthers photographed at the House of Mirrors during the Liège october fair in 1989

References

Surdej, J.: 1990, review paper, Lecture Notes in Physics, Gravitational Lensing, eds Y. Mellier et al., Vol.360, p.57, **"Observational aspects of gravitational lensing"**

Refsdal, S., Surdej, J.: 1992, First invited discourse, XXIst IAU General Assembly, Highlights in Astronomy, ed. J.Bergeron, Vol.9, p.3, **"Gravitational Lensing"**

Refsdal, S., Surdej, J.: 1994, Reports Progress in Physics, Vol.57, 117, **"Gravitational Lenses"**

Surdej, J., Refsdal, S., Pospieszalska-Surdej, A., 1993, 31st Liège International Astrophysical Colloquim, Gravitational Lenses in the Universe, eds J.Surdej et al., p.199, **"The optical gravitational lens experiment"**

Surdej, J., Refsdal, S., Pospieszalska-Surdej, A., 1995, IAU, Symposium No.173, Astrophysical Applications of Gravitational Lensing, eds C.S. Kochanek and J.N. Hewitt, p.417, **"Formation of giant luminous arcs and arclets using an optical gravitational lens experiment"**